Gajo, A., Muir Wood, D. & Bigoni, D. (2007). *Géotechnique* **57**, No. 5, 449–461

On certain critical material and testing characteristics affecting shear band development in sand

A. GAJO*, D. MUIR WOOD† and D. BIGONI*

Laboratory tests on samples of sand typically show instabilities in response related to shear band nucleation and evolution. Influences of constitutive characteristics (for instance, plastically driven elastic anisotropy), sensitivity to changes in constitutive parameters, and effects of testing conditions (for instance, related to stress conditions or to membrane penetration or stretching) on different types of material instability occurring in the post-localisation behaviour of sand specimens are investigated. Comparison between model prediction and available experiments shows that certain constitutive and testing features, which do not much influence the global response of a sample, may nevertheless strongly affect the critical and post-critical behaviours. The results obtained show that the proposed approach is general enough to permit the investigation of effects of experimental features that have not previously been studied.

KEYWORDS: anisotropy; laboratory tests; plasticity; sands; strain localisation

Des essais de laboratoire réalisés sur des échantillons de sable montrent typiquement des instabilités en réponse, liées à la nucléation et l'évolution des bandes de cisaillement. On étudie l'influence des caractéristiques structurales (par exemple, anisotropie élastique d'origine plastique), de la sensibilité aux changements des paramètres de constitution et des effets des conditions de test (par exemple, celles relatives aux conditions de contrainte, à la pénétration de membrane ou à l'étirement) sur les différentes instabilités de matériau se manifestant dans le comportement en post-localisation d'échantillons de sable. La comparaison établie entre le modèle de prédiction et les expériences montre que certains facteurs de structure et d'essai qui n'influent pas significativement sur la réponse globale de l'échantillon peuvent néanmoins avoir une forte influence sur les comportements critiques et post-critiques. Les résultats obtenus indiquent que l'approche proposée est suffisamment générale pour permettre l'étude des effets des conditions expérimentales qui n'avaient pas été examinés jusqu'ici.

INTRODUCTION

Mechanical testing of granular materials frequently reveals instabilities in the form of strain localisation or shear bands that have an important influence on the observed mechanical response. Much analysis of these instabilities has concentrated on the *occurrence* of localisation—the strain conditions at which the instability develops—and the orientation of the subsequent shear band. However, Gajo *et al.* (2004) have used an elastoplastic constitutive framework not only to analyse the onset of shear banding in granular materials but also to support the development of approaches that might be used to describe the post-localisation response. These approaches have led to a new understanding of experimental evidence in granular materials: for instance, it has been explained why particular stress and density states may yield generation of non-persistent shear bands. Moreover, the developed tools have been found to be powerful enough to permit attack on problems not previously studied. Some examples of such problems are considered in this paper. In particular, influences are investigated both of details of the constitutive model and also of features of laboratory testing on initiation of localisation and subsequent response.

The following issues will be addressed.

(*a*) Calibration of a constitutive model is an elaborate *inverse problem* in which values of many constitutive parameters are deduced partly by dissecting individual features of response (such as, for example, aspects of stiffness and strength) and partly by seeking an acceptable quality of visual or mathematical fit to a range of inevitably scattered experimental data. This fit usually concentrates on the global behaviour of homogeneous samples, but the choice of constitutive parameters may have an influence on the expectation of the occurrence of localisation. It will be rare that the selection of parameters will be unique: we explore the *robustness* of the modelling of the occurrence and evolution of localisation linked with changes in model parameters (see 'Sensitivity of strain localisation to selection of constitutive parameters'). For our model, the shear band inclination is shown to be only moderately affected by the choice of constitutive parameters, while the critical strain for occurrence of localisation is found to be much more sensitive.

(*b*) Vardoulakis & Sulem (1995) report extensive analytical studies of constitutive influences on shear band formation, but concentrate on the elements of the description of the plastic properties of the sand. There are several reasons why the modelling of the elastic properties of soils has often been seen as of secondary importance in the development of elastic-plastic soil models: elastic strains are rapidly dominated by plastic strains when medium- to large-strain response in laboratory testing is being simulated; systematic studies of the evolution of elastic stiffness and elastic anisotropy require subtle experimental techniques, which have only become available over the last decade or so; and the development of properly hyperelastic models to describe the observed evolution of stiffness and anisotropy is difficult. However, elastic anisotropy is found to play an important role in the prediction of localisation effects: this is demonstrated later (see 'Effect of elastic anisotropy on biaxial and triaxial tests').

(*c*) Simulation of laboratory tests usually takes at face value the reported elements of stress–strain response, but any

Manuscript received 23 November 2004; revised manuscript accepted 5 January 2007.
Discussion on this paper closes on 3 December 2007, for further details see p. ii.
* Dipartimento di Ingegneria Meccanica e Strutturale, Università di Trento, Italia.
† Department of Civil Engineering, University of Bristol, UK.

laboratory test has boundaries, which in many cases provide only an approximation to the ideal that is sought. For instance, friction on boundaries that are intended to be smooth is known to influence both the homogeneous and the localised response of samples (Desrues *et al.*, 1996); Tatsuoka *et al.* (1990) show that the orientation of bedding planes can have a significant influence on the orientation of shear bands in plane-strain tests on sand. An almost unexplored effect is related to the consequence of having boundaries that are intended to be rigid but actually have a non-zero compliance. This effect and that related to the stretching of the confining membrane during post-critical behaviour are analysed later (see 'Effects of membrane constraints'). It is shown that, while the effect of the membrane is second-order so far as homogeneous stress–strain behaviour is concerned, the membrane interactions may have a marked influence on the detail of the localisation and post-localisation response.

The theoretical background to the analysis of localisation is reported in detail by Gajo *et al.* (2004); the constitutive model has been described in Gajo & Muir Wood (1999a, 1999b): these will not be repeated here. In contrast, we shall endeavour to present the essential concepts of the constitutive modelling (see 'Outline of constitutive model') and localisation studies (see 'Mechanisms of localised deformation of sand') through diagrams and descriptions, confining the relevant equations to the Appendix. Results presented in the subsequent sections may stimulate further experimental studies.

OUTLINE OF CONSTITUTIVE MODEL

The analyses that are reported here have made use of a particular constitutive model, which is a variant of Severn-Trent sand (Gajo & Muir Wood, 1999a, 1999b), but it is considered unlikely that the conclusions will be specific to that model. A general description of the model will be given here; more detail can be found in those references and in Gajo *et al.* (2004). A pictorial presentation is provided below, and a brief mathematical presentation of the model is given in the Appendix. Although particular equations are suggested for the lines sketched in Figs 1–3, and these have been used in the implementation of the model, the lines are intended to indicate that in each case some assumption about the link between the pairs of variables needs to be made; the model used here has tried to use simple forms.

The model is essentially a generalisation of a Mohr–Coulomb elastic-isotropic hardening plastic model, based on a smooth yield surface (Fig. 1(a)). The strength of the soil is purely frictional in origin, but it is assumed that the current strength depends on the current density of packing and stress level through the so-called *state parameter* ψ (Fig. 1(b)), which is the distance, in terms of specific volume v, of the current state of the soil (specific volume and mean effective stress p') from the critical state for the same mean effective stress (Wroth & Bassett, 1965; Been & Jefferies, 1985). The model thus requires some experimentally informed description of this critical state line: for example, its slope Λ and intercept v_Λ (Fig. 1(b)).

The current strength surface (in a principal stress representation) is assumed to be a function of the current state parameter ψ (Figs 1(c), 1(d)), through the critical state strength ϕ_{cs} and a controlling constitutive constant k. At any instant, the deviatoric strength criterion has the 'curved triangular' form (shown in Fig. 1(c)) described by a function $g(\theta_{(\sigma)})$ of Lode angle $\theta_{(\sigma)}$. This function is sufficiently constrained by a constant m that defines the ratio of strengths in triaxial extension and triaxial compression.

The ratio of current *mobilised* strength to current *peak* strength is assumed to be a monotonic hyperbolic function of plastic distortional strain (Fig. 1(e)): this function introduces a constitutive constant B, taking large values for low plastic stiffness.

The yielding of the material is governed by the current mobilised strength (Fig. 1(a)), but the plastic dilatancy (the ratio of plastic incremental volumetric strain to plastic incremental distortional strain) is governed by a Cam-clay type flow rule (Fig. 1(f)) so that the flow is non-associated. This flow rule introduces a constitutive constant A that modifies the dilatancy when the current mobilised strength is different from the critical state strength, and also a constant k_d introducing a dependence of plastic dilatancy on the state parameter ψ.

The operation of this constitutive model can be simply summarised. Although the distortional hardening relationship in Fig. 1(e) is monotonic, it describes the development of the ratio of a currently mobilised strength to a currently available peak strength. That current peak strength is a function of stress level and density (Fig. 1(d)) through the state parameter (Fig. 1(b)). The flow rule (Fig. 1(f)) leads to changes in density towards the critical state whenever plastic distortional strain occurs. Change in density leads to change in currently available peak strength. Because of the asymptotic nature of the hardening relationship (Fig. 1(e)), the available strength can be attained only at large distortional strain, by which time it has become identical with the critical state strength. The model is thus able to predict strain-softening for dense sands in spite of the monotonic hardening relationship (Fig. 1(e)). This potential strain-softening will be apparent in some of the simulations that will be presented.

Experimental evidence of the existence of a finite elastic region is complicated by the circumstance that under monotonic loading the elastic deformation is rapidly swamped by the plastic deformation. However, an elastic range is postulated in our model, and an underlying elastic description is required for stress reversals and stress states that lie inside the yield surface. The simplest form of elastic model would use isotropic elasticity, with a shear stiffness μ and Poisson's ratio ν. Pragmatically, because the model assumes a *finite* size of elastic region at all times, the shear stiffness has been taken as a reduced multiple of the *zero strain* stiffness μ_0, which can be calculated using empirical expressions such as that presented by Hardin & Black (1968). Alternatively, it might be recognised that the elasticity of soils is anisotropic, and that the nature of this anisotropy is not constant but evolves with history as a function of the current fabric of the soil (e.g. Muir Wood *et al.*, 2001). Gajo *et al.* (2001) and Gajo (2004) reported experiments in which dense and loose samples of Hostun sand were subjected to small undrained unload–reload cycles, starting from different points on known drained stress paths, and observed that one interpretation of the varying slope β of these stress path cycles (Fig. 2(a))[1] is an evolving anisotropy of elastic stiffness with plastic distortional strain (Fig. 2(b)) with the degree of anisotropy *saturating* as the strain increases, and with the horizontal stiffness eventually becoming almost negligible by comparison with the vertical stiffness.[2] This

[1] The test from which β has been evaluated in Fig. 2(a) follows a stress path that starts from a state of triaxial extension, and β is found to be initially negative. Parameter β changes sign (becoming positive) during the compression part of this stress path. However, the results shown in Fig. 2(b) refer to a test with monotonic loading starting from a null deviatoric stress.

[2] An alternative interpretation through stress-dependent non-linearity (Houlsby, 1985) appears to be less well supported by the experimental observations.

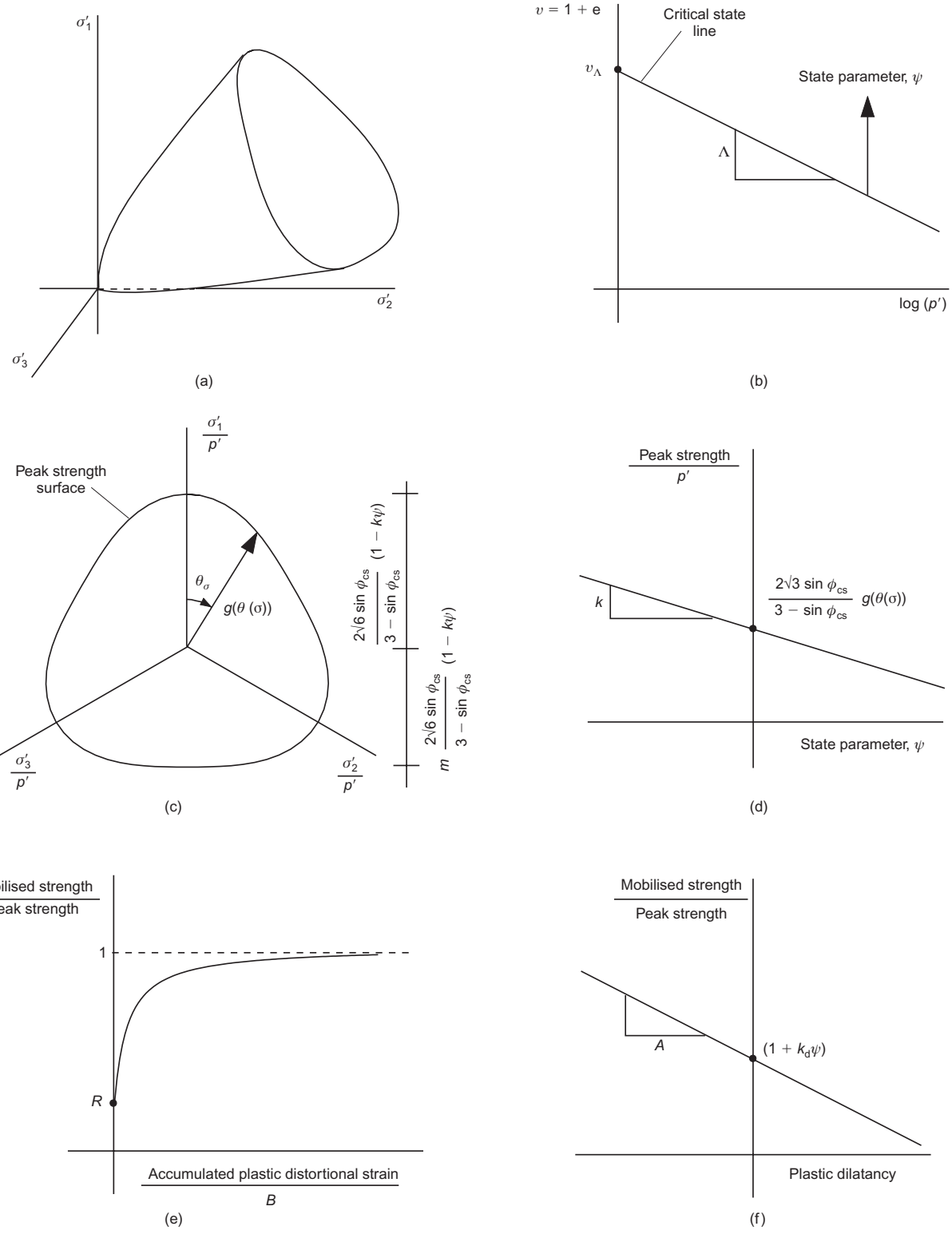

Fig. 1. Elements of constitutive model and definition of constitutive parameters: (a) yield surface; (b) definition of state parameter ψ and critical state line (v_Λ, Λ); (c) deviatoric section of peak strength surface and indication of role of m; (d) dependence of current peak strength on state parameter and introduction of critical state friction angle ϕ_{cs} and parameter k; (e) monotonic hyperbolic variation of ratio of *current* mobilised strength to *current* peak strength with accumulated plastic distortional strain normalised with plastic stiffness parameter B; (f) dependence of plastic dilatancy on mobilised strength and indication of role of A and k_d

experimental evidence has been modelled by a second-order (positive definite) fabric tensor **B** in the way shown by Bigoni & Loret (1999) and Gajo *et al.* (2004) and summarised in the Appendix. The fabric tensor depends upon the plastic strain, so that an evolving anisotropy is described within the framework of elasto-plastic coupling (Hueckel & Maier, 1977). The three parameters defining the fabric tensor are: A_ε, describing the asymptotic value of anisotropy in triaxial compression, Fig. 3(a); B_ε, which, similar to B (Fig. 1(e)), describes the rate at which anisotropy develops with increasing distortional plastic strain (Fig. 3(b)); and m_ε, which controls the ratio of the asymptotic values of anisotropy that can be attained in triaxial extension and triaxial compression (Fig. 3(a)). Experimental results shown in Fig.

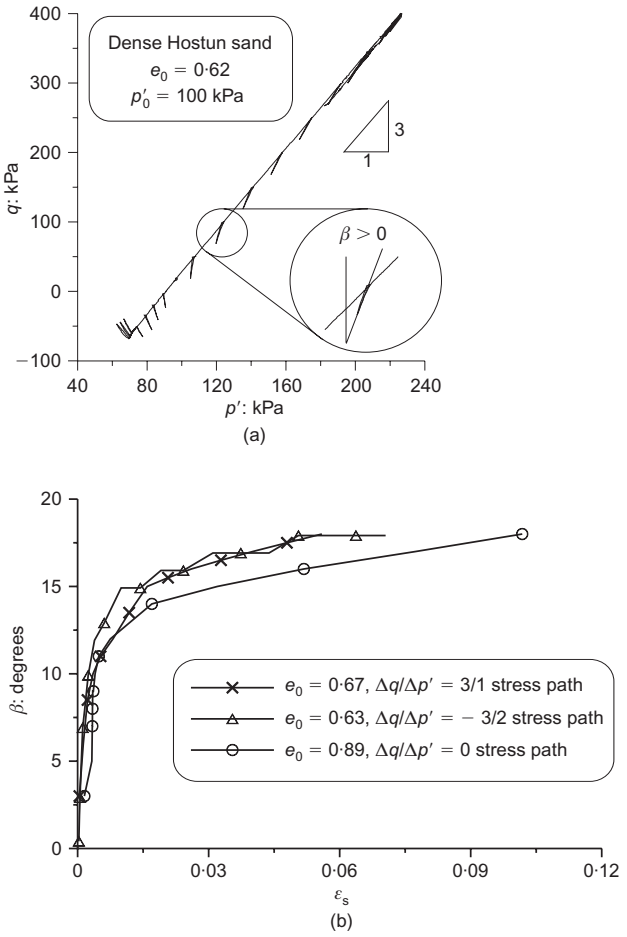

Fig. 2. Experimental exploration of evolution of tangent elastic anisotropy in triaxial tests: (a) conventional drained test with initial extension stress state and definition of inclination β of effective stress path resulting from a small undrained unload–reload cycle; (b) evolution of tangent elastic anisotropy β with deviatoric strain for loose and dense sand along different compression loading paths

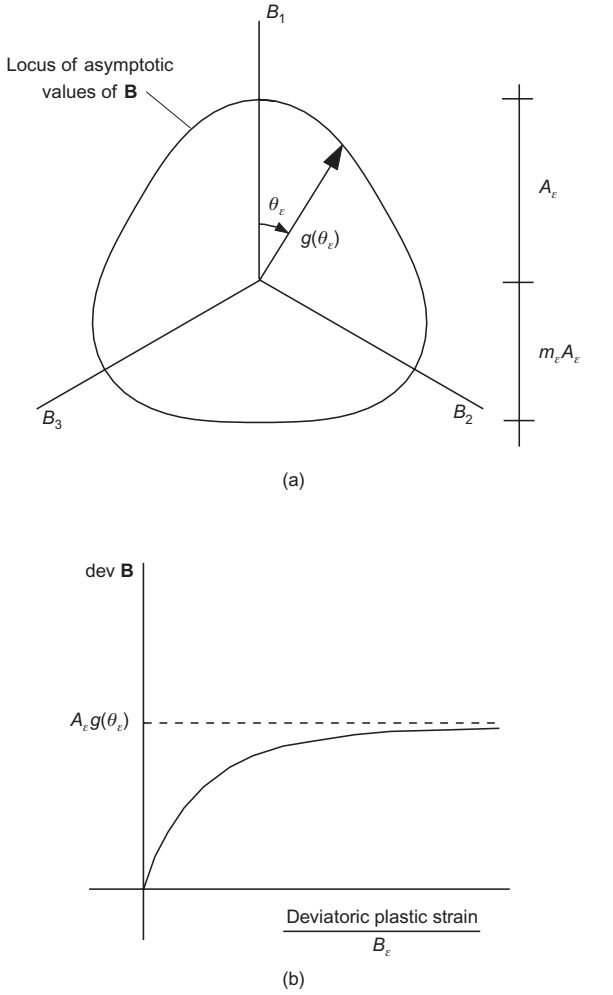

Fig. 3. Elements of evolution of fabric tensor B defining elastic anisotropy and definition of corresponding constitutive parameters: (a) locus of asymptotic values of B in deviatoric plane; (b) monotonic variation of deviatoric component of B with deviatoric plastic strain with controlling parameter B_ε and asymptote A_ε

2 have been used to calibrate A_ε and B_ε, while m_ε has been determined on the basis of experiments performed in triaxial extension (Gajo, 2004). While the evolution of elastic anisotropy is calibrated against the evolution of β seen in axisymmetric triaxial tests, the evolving fabric tensor is linked to the evolving plastic distortional strain, and is not constrained by any artificial symmetries. Although this description of anisotropy—and the inspiring experimental data—have come from axisymmetric triaxial tests, the formulation is thus entirely general (Gajo *et al.*, 2004) and merely awaits additional experimental data for its refinement.

Illustration of the second-order significance of incorporating the evolution of anisotropy in the elastic formulation in matching monotonic triaxial compression data is provided in Fig. 4: the quality of the simulation is somewhat unchanged.

Figure 5 explores another effect relating to selection of parameters. There is always an element of subjectivity in making a final choice of parameters, because it will never be possible to obtain an exact match to all the available experimental data.

The parameters that give the best match over strains up to, say, 20% may well not be the ideal set to describe the early response over a much smaller strain range. Gajo (2003) shows that the model is quite sensitive to imposed strain constraints: matching data from undrained tests or biaxial (plane strain) tests is more difficult than drained triaxial tests. The shear deformations are controlled primarily by the shear modulus μ and the parameter B, which is essentially a plastic compliance. Fig. 5 compares simulations made with $B = 0{\cdot}004$ and $\mu = \mu_0/5$ and with $B = 0{\cdot}0012$ and $\mu = \mu_0/2{\cdot}5$. The former are quite good over a wide range of axial strains, whereas the latter lead to a stiffer stress–strain response that better matches the initial soil response. This latter set (in which both elastic and plastic stiffnesses have been increased) is found to give a good simultaneous match to drained and undrained tests (see Gajo, 2003, for details).

MECHANISMS OF LOCALISED DEFORMATION OF SAND

The simulations shown in Figs 4 and 5 assume that homogeneous response of the soil sample can be maintained to substantial strains even in the presence of a more or less significant peak in the stress–strain response. The analyses reported by Gajo *et al.* (2004) investigate the possibilities for a bifurcation from this homogeneous response and the resultant formation of a shear band of localised deformation. The analysis of strain localisation initiation is performed in a standard way following concepts introduced by Bigoni *et al.* (2000). The post-localisation analysis, described in detail by Gajo *et al.* (2004), is performed as follows.

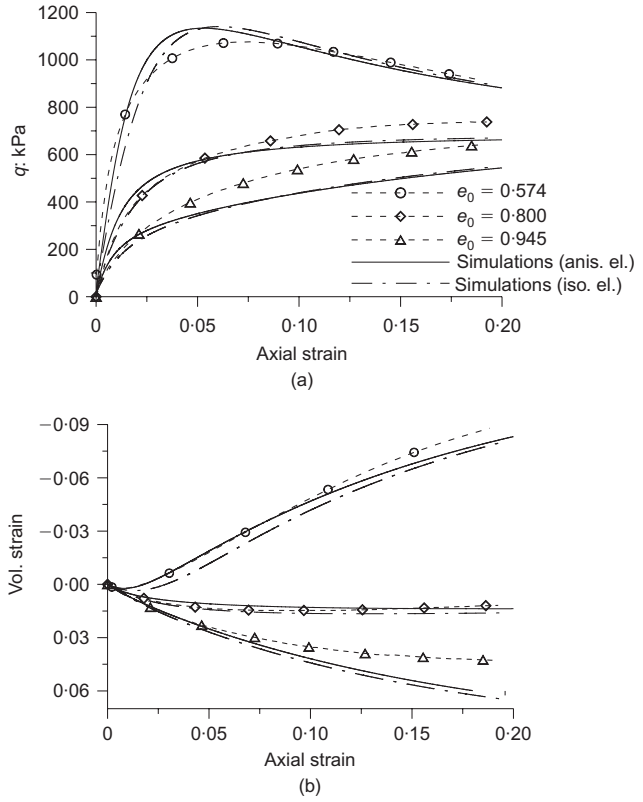

Fig. 4. Drained, conventional triaxial compression tests on Hostun sand RF (initial pressure $p'_0 = 300$ kPa): experiments and simulations. Comparison of isotropic and anisotropic elasticity: (a) deviatoric stress and axial strain; (b) volumetric and axial strain

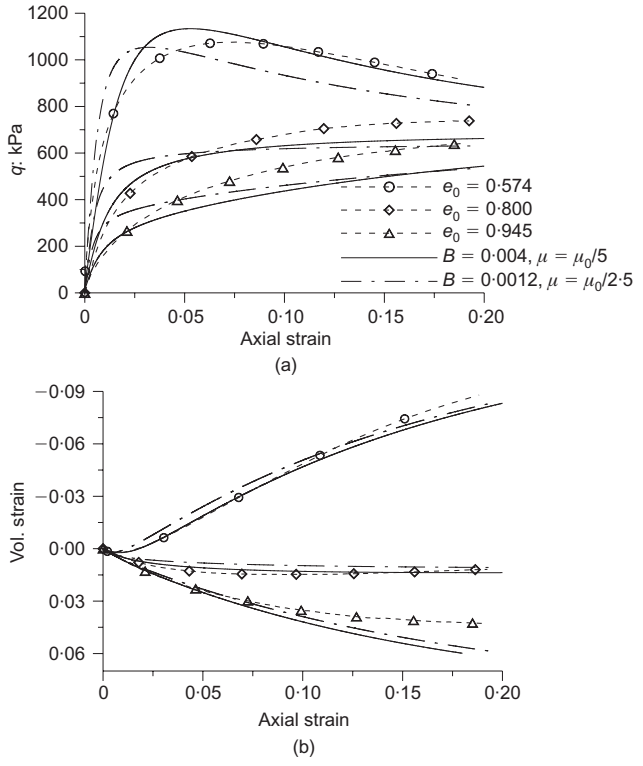

Fig. 5. Drained, conventional triaxial compression tests on Hostun sand RF (initial pressure $p'_0 = 300$ kPa): experiments and simulations. Effect of choice of constitutive parameters: (a) deviatoric stress and axial strain; (b) volumetric and axial strain

(*a*) A constant thickness is assigned to (not calculated for) the shear band. (On the basis of experimental results, the shear band thickness is assumed equal to 15 times the mean grain diameter, following Roscoe (1970) and Muir Wood (2002).)

(*b*) A homogeneous response is assumed not only before shear banding but also outside and inside the shear band after shear banding.

(*c*) Equilibrium, strain compatibility, elastic unloading and plastic loading are checked during a step-by-step numerical integration.

(*d*) The 'observed externally' vertical displacements (hence 'conventional' strain) is computed as the sum of the contributions of the responses within and outwith the shear band.

Figure 6 shows the three different possibilities that have been identified for the post-localisation response, in each case showing what would be observed externally for the stress–strain response calculated ignoring the internal heterogeneity of the sample.

The dense sample tested at a high stress level ($e_0 = 0·673$, $p'_0 = 400$ kPa, label 'DS1') shows the expected bifurcated response with localisation occurring before the peak of the homogeneous response (a consequence of the assumption of non-associated plastic flow) followed by a rapid drop of stress to a residual value.

The dense sample tested at a lower stress level ($e_0 = 0·673$, $p'_0 = 20$ kPa, label 'DS2') and the loose sample ($e_0 = 0·914$, $p'_0 = 100$ kPa, label 'LS') show a response that we have described as *band saturation* (Gajo *et al.*, 2004).[3]

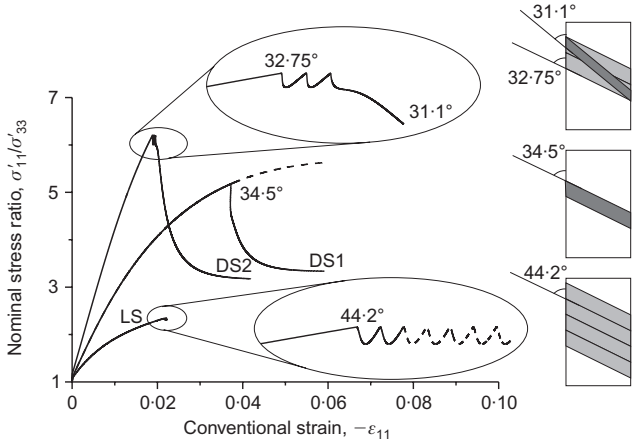

Fig. 6. Three mechanisms of localised deformation in sand: simulations of the 'global' compression response of a 350 mm high biaxial sample of dense sand at high confining pressure ($e_0 = 0·673$, $p'_0 = 400$ kPa, label 'DS1'), at low confining pressure ($e = 0·673$, $p'_0 = 20$ kPa, label 'DS2'), and of loose sand ($e_0 = 0·914$, $p'_0 = 100$ kPa, label 'LS'). Formation of a single shear band is observed in DS1, whereas non-persistent and persistent band saturation are exhibited in DS2 and LS respectively

[3] Band saturation (as sketched in the details of Fig. 6) consists in a drop in the nominal stress ratio, followed by a re-hardening. *Qualitatively, but not quantitatively*, this mechanism is similar to the experimentally observed rise in the nominal stress ratio at larger strain shown in Fig. 7. Our simulations will show that the two phenomena are quite different: the former is a material response for a given stress path (Gajo *et al.*, 2004), while the latter is a system response resulting from membrane stretching (so that it is an experimental artefact: see 'Effect of membrane constraints'). From an experimental point of view, band saturation could be discriminated from membrane stretching (a) because the associated deformations during band development are small (as in Fig. 6), and (b) by referring to samples of different (out-of-plane) thickness.

In the analyses, when localisation occurs, the soil inside the shear band continues to deform plastically while the soil outside the shear band unloads elastically, maintaining compatibility of stresses and strains at the boundary between plastic and elastic material. The constitutive model describes continuing changes in density, and hence in available strength and dilatancy, within the shear band. In the cases labelled 'DS2' and 'LS' the overall, global response changes from softening to hardening until a second shear band occurs in the material that, subsequent to the previous localisation, had been unloading elastically and is now again at yielding. This process of successive repeated shear band formation is *band saturation*. When sufficient shear bands have thus formed it may be possible for a new band to form at a different angle within the collection of prior shear bands, assumed contiguous. This new band may then lead to global softening ($e_0 = 0{\cdot}673$, $p'_0 = 20$ kPa, label 'DS2') or further band saturation ($e_0 = 0{\cdot}914$, $p'_0 = 100$ kPa, label 'LS') (Fig. 6).

Some of the experimental observations that have been interpreted by Gajo *et al.* (2004) as indicating the occurrence of band saturation are shown in Fig. 7 (Desrues & Hammad, 1989). For the loose sand, the measurement of band inclination (27·5°) is believed to be less accurate than that performed using stereophotogrammetric techniques by Finno *et al.* (1997) and Chambon & Desrues (1986), who observed inhomogeneity of local strain supporting the presence of a persistent process of band broadening in loose sand samples.[4] However, the global stress–strain curve for loose sand shown in Fig. 7 is considered representative and can be compared with the simulations of Fig. 6, supporting the hypothesis underpinning the theoretical finding that the observed plateau of stress–strain response is the result of a persistent process of band saturation.

Experimental evidence of band saturation in dense sand at low confining pressures is believed to be missing because it is expected to occur at negligible confining pressures (lower than the pressures that are usually investigated), to be non-persistent, and to be delayed by the out-of-plane compliance (see 'Effects of membrane constraints'). For the dense sand, the computed band inclinations agree moderately well with observations only at large confining pressures: the computed bands are more nearly horizontal than the observed bands at low confining pressures. In fact, the computed inclinations seem to be closer to the 'Roscoe' orientation, controlled by the dilatancy of the sand, whereas the observed inclinations seem to be closer to the 'Coulomb' orientation, controlled purely by the stress state in the sand (Vardoulakis & Sulem, 1995). This discrepancy evidently calls for further investigation.

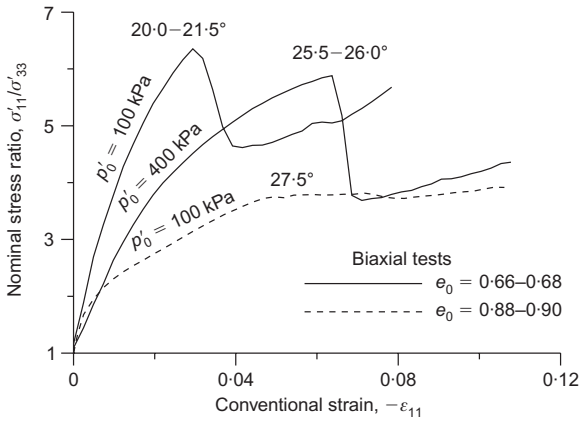

Fig. 7. Experimental results for compression of 350 mm high biaxial samples of dense and loose sand at different confining pressures (results taken from Desrues & Hammad, 1989)

[4] Note that in the experimental setting used by Finno *et al.* (Chambon & Desrues, 1986) the bottom (top) of the samples was free to slide (and rotate) horizontally. Therefore band saturation cannot be ascribed to a re-hardening effect due to boundary restraint.

Desrues & Viggiani (2004) do not directly present results of photogrammetric measurements that support the possibility of the occurrence of band saturation. However, they mention that 'shear band formation is progressive [and ...] patterns of deformation are not necessarily simple. Temporary modes of localised strain [are visible ...] prior to the developments of a final persistent band.' They also note that 'temporary or non-persistent modes of localisation [...] eventually disappear.' Desrues (1984) mentions the appearance of a second shear band, occurring after a second peak in the force–displacement diagram is reached. Photogrammetric evidence of non-persistent shear bands has been given by Finno *et al.* (1997).

The constitutive and testing variations that are being explored in this paper will now be presented in terms of their effect on the character of the post-localisation response as well as on the details of the occurrence of localisation: the angle of the shear band (Fig. 6) and the axial strain at which it develops.

SENSITIVITY OF STRAIN LOCALISATION TO SELECTION OF CONSTITUTIVE PARAMETERS

In order to quantify the influence of the individual constitutive parameters on the onset of strain localisation, we have performed a parametric analysis in which each parameter was varied in turn from the following calibrated values (given by Gajo *et al.*, 2004):

$$\phi_{cs} = 32°,\ m = 0{\cdot}80,\ B = 0{\cdot}004,\ A = 0{\cdot}6,\ k = 2{\cdot}5,$$
$$\nu = 0{\cdot}1,\ \mu = \mu_0/5{\cdot}0,\ k_d = 2{\cdot}2,\ A_\varepsilon = 1{\cdot}10,\ m_\varepsilon = 0{\cdot}45,$$
$$B_\varepsilon = 0{\cdot}020 \qquad (1)$$

Results of this analysis are summarised in Table 1, in which attention is concentrated on the band inclination (second column) and on the magnitude of vertical strain at which localisation occurs (third column) for a drained biaxial compression test at a confining pressure of $p'_0 = 400$ kPa, performed on dense Hostun sand ($e_0 = 0{\cdot}673$). The values of the parameters varied in the analyses are reported in the first column, while all the others have been taken fixed.

It can be observed that even large variations of the

Table 1. Effects of variation of each constitutive parameter on band inclination and axial strain at the onset of strain localisation. Results obtained for $e_0 = 0{\cdot}673$ and $p'_0 = 400$ kPa.

	Band inclination	Conventional axial strain at localisation
Reference calibration	34·5°	3·72%
$\phi_{cs} = 33°$	34·2°	3·83%
$m = 0{\cdot}85$	34·4°	4·08%
$B = 0{\cdot}006$	34·9°	4·24%
$A = 0{\cdot}9$	33·7°	3·75%
$k = 3{\cdot}0$	34·0°	3·74%
$\nu = 0{\cdot}2$	34·5°	3·10%
Isotropic elasticity	35·4°	4·40%
$\mu = \mu_0/2{\cdot}5$	35·7°	2·53%
$k_d = 1{\cdot}0$	35·1°	3·80%
$A_\varepsilon = 1{\cdot}43$	33·7°	3·66%
$m_\varepsilon = 0{\cdot}59$	34·2°	3·75%
$B_\varepsilon = 0{\cdot}014$	34·4°	3·69%

constitutive parameters lead to negligible variations of band inclination, the range of which is just 2° (between 33·7° and 35·7°). In contrast, the range of variation of axial strain at the initiation of strain localisation is much wider: from 2·53% to 4·40%. The major effects are associated with the choice of isotropic or anisotropic elasticity and with the detail of elastic stiffness, taken equal[5] to $\mu = \mu_0/5{\cdot}0$ and $\mu = \mu_0/2{\cdot}5$.

A more detailed analysis of the effects induced by elastic and plastic stiffness on the onset of strain localisation and on the post-localisation regime is given in Fig. 8, which shows the comparison between the simulations obtained with the constitutive parameters given in list (1) and the alternative choice of constitutive parameters used in Fig. 5, where the plastic and elastic stiffnesses have been increased in order to improve the simulation of the response at small strains. The simulations refer to drained biaxial tests on dense Hostun sand at confining pressures of $p'_0 = 100$ kPa and $p'_0 = 400$ kPa. The effect on volumetric response in these plane strain tests (Fig. 8(b)) is somewhat greater than for the triaxial tests (Fig. 5(b)) because of the additional kinematic constraint provided by the imposed plane strain condition. However, while both sets of parameters can be justified in their ability to match certain features of the stress–strain response, it is demonstrated in Fig. 8 that the effect on the localisation and post-localisation response can be quite significant. The stiffer elastic and plastic response ($\mu = \mu_0/2{\cdot}5$, $B = 0{\cdot}0012$) makes band localisation appear at much smaller axial strains, and induces band saturation at larger confining pressure ($p'_0 = 100$ kPa instead of $p'_0 = 20$ kPa). The effect on band inclination is small (approximately 1°) and, for both stiffness values, an increase of confining pressure leads to a decrease of band inclination, as observed experimentally (see e.g. Desrues & Hammad, 1989).

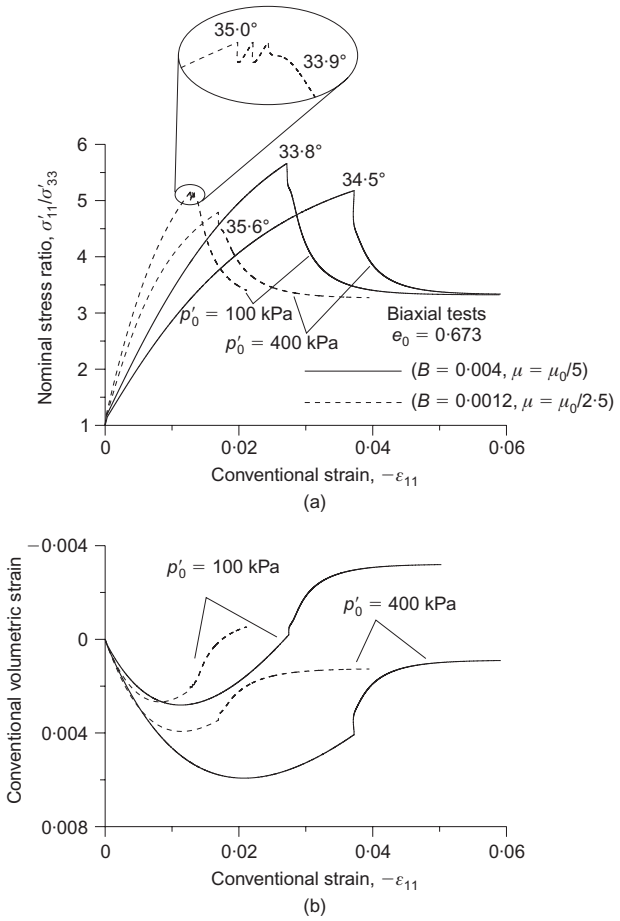

Fig. 8. Effects of choice of constitutive parameters on occurrence of strain localisation in drained biaxial compression tests performed at various confining pressures on dense sand: (a) nominal stress ratio against conventional axial strain; (b) conventional volumetric strain against axial strain

[5] In each simulation of the biaxial test the constant value of elastic shear modulus μ_0 at small strain was obtained considering a mean pressure equal to three times the confining pressure (i.e. $p' = 3p'_0$) in the Hardin & Black (1968) expression, representative of the mean value of pressure imposed during the test.

In conclusion, different values of constitutive parameters that lead to plausible simulations of triaxial test response—especially sets of parameters chosen to improve the match over particular regimes of observation—can lead to large variations of stress–strain response and of post-critical response for biaxial simulations. On the other hand, the band inclination is scarcely affected by the different choices of constitutive parameters.

Once localisation of shear deformation occurs, the volumetric strains averaged globally over the entire sample are no longer representative of the volumetric strains occurring in the region of continuing shearing: the shear band. Desrues *et al.* (1984) show void ratio evolution within shear bands detected using radiography, and show how these local void ratios appear rapidly to move towards a critical state—much as shown by the marked transition in volumetric response seen after the occurrence of localisation in the simulations of Fig. 8 (and Figs 10, 14 and 17)—whereas the overall averaged volumetric response is much less ordered.

The simulations of tests on dense sand reported here show somewhat reasonable correspondence of volumetric strains prelocalisation but lower volumetric dilatancy after localisation than is seen in the biaxial experiments, whereas volumetric strains in the calibration triaxial tests are well matched (Figs 4 and 5). Gajo *et al.* (2004) show closer agreement for volumetric strains in simulations of biaxial tests on loose sand. There are a number of constitutive effects that could influence this result; however, the focus in this paper is on the effects of localisation on the observed shearing response.

EFFECT OF ELASTIC ANISOTROPY ON BIAXIAL AND TRIAXIAL TESTS

Although elastic anisotropy has been shown to have negligible influence on the simulation of monotonic shearing (Fig. 4), the effect on modelling strain localisation occurring in drained triaxial compression tests in sand can be important. The simulated homogeneous stress–strain behaviour for a drained triaxial compression test on a dense sand sample ($e_0 = 0{\cdot}60$) at low confining pressure ($p'_0 = 60$ kPa) is shown in Fig. 9(a) (compare Fig. 4). The onset of localisation is deduced in analysis by comparison of the hardening modulus H (positive for hardening, negative for softening and null for perfectly plastic behaviour: see the Appendix for its mathematical definition) with the critical value of the hardening modulus H_{crit} which leads to singularity of the acoustic tensor and hence to the possibility that localisation will occur. The evolution of values of H and H_{crit} with axial strain is shown in Fig. 9(b). Results obtained neglecting evolution of elastic anisotropy (and thus corresponding to isotropic elasticity) are shown with a dashed line, while the solid line corresponds to the full anisotropic version of the model.

Because the stress–strain responses in Fig. 9(a) are closely similar for the isotropic and anisotropic elastic models, the values of H in Fig. 9(b) are essentially identical. The values of the critical hardening modulus H_{crit} are, however,

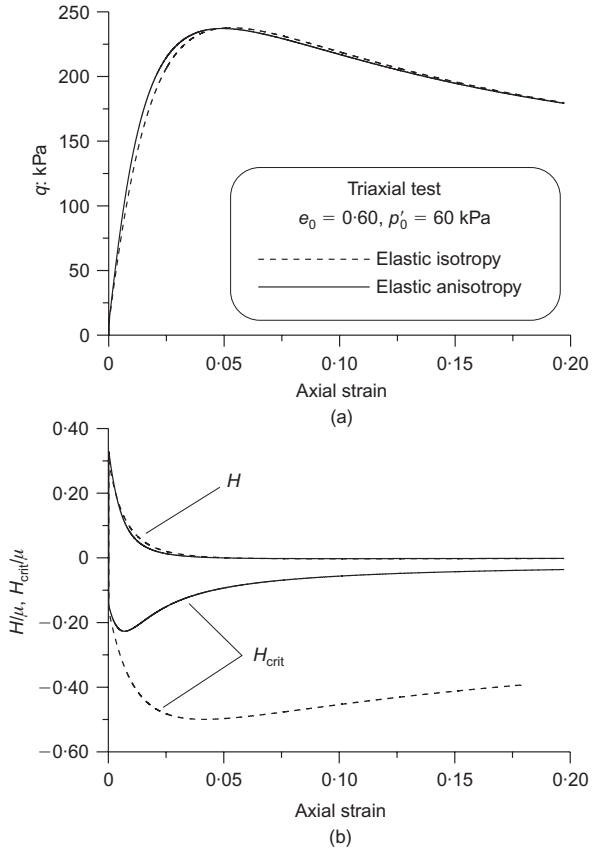

Fig. 9. Effects of elastic anisotropy on occurrence of strain localisation in a drained triaxial compression test on dense sand: (a) stress–strain behaviour; (b) evolution of hardening modulus for material, and critical hardening modulus for localisation

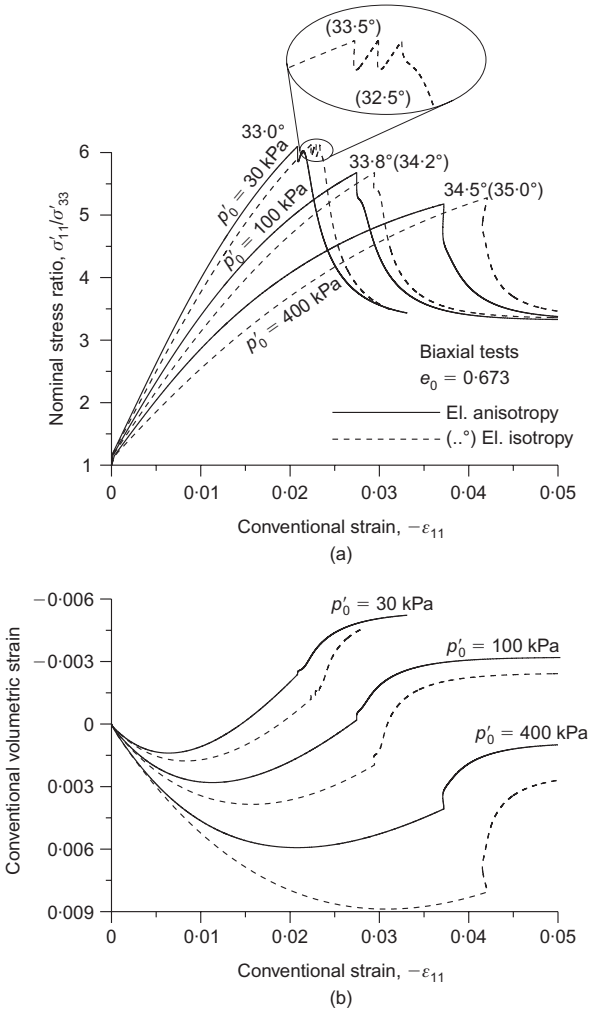

Fig. 10. Effects of elastic anisotropy on occurrence of strain localisation in drained biaxial compression tests performed at various confining pressures on dense sand: (a) nominal stress ratio against conventional axial strain; (b) conventional volumetric strain against axial strain

quite different. Over the range of deformations considered, the value of the hardening modulus H never reaches the critical value H_{crit} for either model, but the difference between the two values for the anisotropic elastic model is so small that an appropriate small perturbation may induce strain localisation, whereas this will not occur for the isotropic elastic model. The fact that the values of critical and material hardening moduli are almost parallel and close to each other for a wide range of deformation makes the problem very sensitive to imperfections. This may correspond to the dispersion of the data relative to the critical deformations for strain localisation observed by Desrues *et al.* (1996), who found, using tomographic analysis, that the initiation of strain localisation could occur at axial strains ranging between 16% and more than 19% in triaxial tests performed with lubricated ends, on Hostun sand at similar confining pressure and void ratios. We reiterate that elastic anisotropy has no practical influence on the stress–strain behaviour shown in Fig. 9(a), but it has a very significant effect on the critical hardening modulus shown in Fig. 9(b), a circumstance in agreement with findings by Bigoni & Loret (1999).

The effects induced by elastic anisotropy on drained biaxial tests are presented in Fig. 10. The results reported were obtained with isotropic and anisotropic elasticity using the values of the constitutive parameters given in list (1). The simulations refer to drained biaxial tests on dense Hostun sand at confining pressures ranging between $p'_0 = 30$ kPa and $p'_0 = 400$ kPa. Elastic isotropy is more prone than anisotropic elasticity to induce band saturation at low confining pressure. In fact, with isotropic elasticity band saturation occurs at slightly larger confining pressure ($p'_0 = 30$ kPa instead of $p'_0 = 20$ kPa for elastic anisotropy). However, the effects of elastic anisotropy increase with the increase of confining pressures. Even in the range of axial strains in which the sample is still homogeneous the differences are large (much larger than those obtained in triaxial tests, in Fig. 9), again because of the additional kinematic constraint imposed by the plane-strain configuration. The differences become larger when strain localisation occurs, because elastic isotropy induces strain localisation at larger axial strains. Finally, we note that elastic anisotropy induces a remarkable decrease of volumetric compressive strain.

EFFECTS OF MEMBRANE CONSTRAINTS

The purpose of this section is to show that details of the experimental set-up—for instance, characteristics of the boundary conditions—may, when modelled, yield unexpectedly relevant results. One of these, related to membrane penetration by the sand grains, merits a detailed exploration since the soil–membrane interaction has a significant effect on the out-of-plane state of stress in the material during a nominally plane strain test.

In the usual experimental set-up for biaxial tests, the sand sample is confined between two thick glass plates, to simulate a plane-strain condition. However, there is a rubber membrane (lubricated with silicone grease) separating the sand from the glass (Fig. 11). While the glass might be

assumed infinitely rigid, this is not true for the membrane. It is reasonable to expect that the sand grains will penetrate into the membrane, so that there is a certain finite out-of-plane compliance. Thus, while an overall plane strain constraint is imposed at *system* level, the soil sample itself is able to experience a departure from the plane-strain condition.

The exact evaluation of this out-of-plane compliance is a hard task, since at a micromechanical level the grains are not all uniformly loaded as the sample is deformed, but chains of highly loaded grains are formed (e.g. Drescher and de Josselin de Jong, 1972). As a result, the grains belonging to these chains penetrate into the membrane rather independently as if they were not interacting with each other. In order to provide an *order of magnitude* estimate for this compliance, we have performed a few finite element simulations using ABAQUS standard[6] (v. 6·1; Hibbitt, Karlsson and Sorensen Inc, Pawtucket, RI), considering a large-strain analysis of the penetration of a rigid sphere (having a mean diameter equal to the mean diameter of the Hostun sand grains, $D_{50} = 0{\cdot}38$ mm) into a 0·50 mm thick, neo-Hookean, incompressible, elastic support (with an initial elastic modulus $E = 1000$ kPa), bounded by a cylindrical smooth surface having a diameter of 1·6 times larger than the mean diameter of the sand grains, playing the role of a representative cell at the inhomogeneous sand/rubber contact.[7] Fig. 12 shows the undeformed and deformed finite element meshes. The value of the diameter of the cylindrical boundary of the numerical model obviously has a major effect on the computed compliance for the penetrating sphere. However, the influence of this boundary diameter on the out-of-plane compliance changes non-linearly as it is increased further. Though not based on actual observation of particle chain separation from photoelastic or distinct element modelling,[8] the value selected provides a simple estimate of this compliance, which is almost certainly underestimated (owing to the over-stiff lateral boundary conditions assumed for the representative cell). If in fact the stress is transmitted through the sand by chains of particles with a spacing of, say, 5–10 times particle diameter (such a spacing seems a typical outcome of many analyses), then the resulting compliance will be even higher and the influence on the localisation and post-localisation behaviour correspondingly greater.

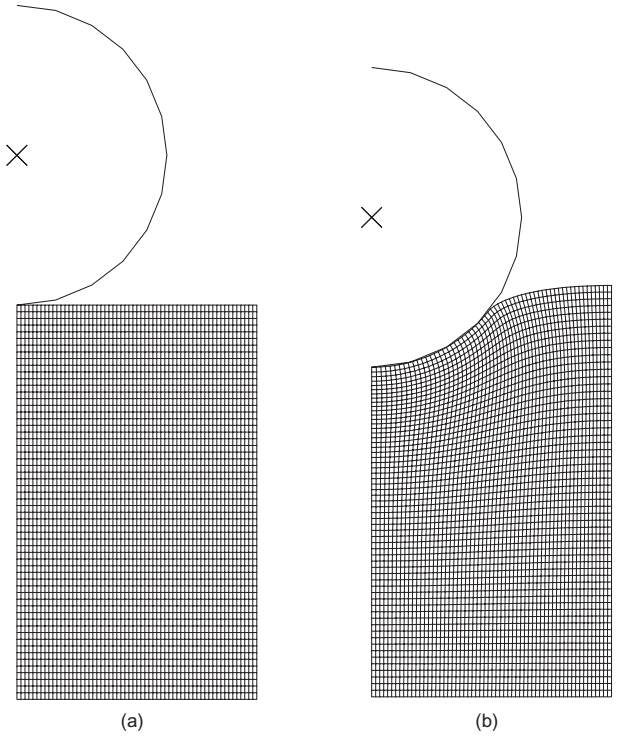

Fig. 12. (a) Undeformed and (b) deformed finite element mesh employed for evaluating penetration of rigid sphere of diameter 0·38 mm into 0·50 mm thick, neo-Hookean, incompressible, elastic support, with smooth constraint on lateral and bottom surfaces

The out-of-plane effective stress σ'_{22} may be deduced by averaging the punching force F_c (evaluated from the ABAQUS simulation) over the area of the model associated with each individual particle. The results of the finite element simulation, interpreted in this way, are summarised in Fig. 13: the out-of-plane compliance is seen to be strongly non-linear. In particular, the interpolation law shown in Fig. 13 can be written as the following polynomial expression in terms of the membrane penetration δ_3 (expressed in mm)

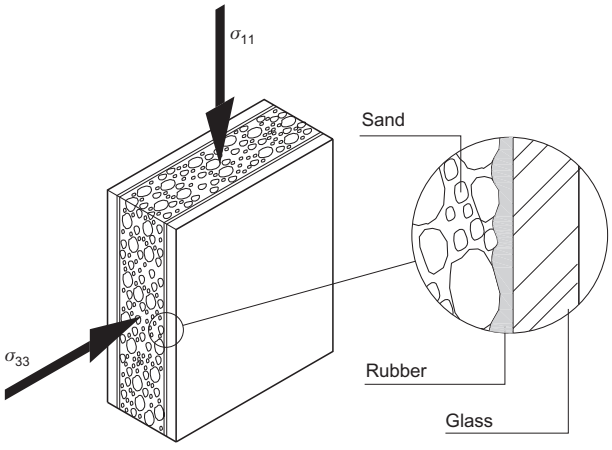

Fig. 11. Experimental arrangement for plane-strain tests

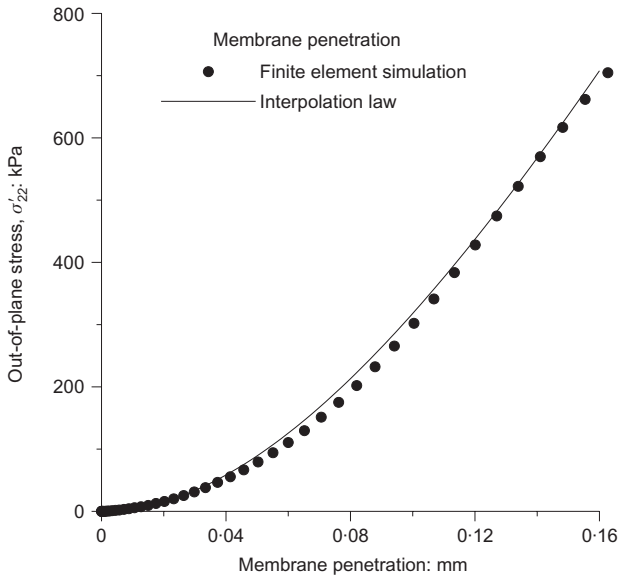

Fig. 13. Out-of-plane stress as a function of membrane penetration evaluated through finite-element modelling (Fig. 12)

[6] Four-noded, axisymmetric, bilinear hybrid elements (CAX4H) with constant pressure have been employed, with a mesh of 60 × 60 elements.

[7] For comparison, for a body-centred cubic arrangement of regular spheres the spacing of the spheres along an edge of the cubical unit cell is 1·15 diameters and across a basal diagonal 1·63 diameters.

[8] Most photoelastic or distinct element observations have been presented for rigid kinematically controlled boundaries and have not explored the effect of a compressible external boundary resulting, as here, from membrane compliance.

$$\sigma'_{22} = 40000\ \delta_3^2 - 90000\ \delta_3^3 + 80000\ \delta_3^4 \qquad (2)$$

where σ'_{22} is taken positive when compressive and expressed in kPa. The out-of-plane stress is only defined for positive values of the membrane penetration.

Localisation analyses have been performed, accounting now for the non-linear out-of-plane stiffness given by equation (2). The out-of-plane compliance influences both the onset of localisation and the post-localisation behaviour. Obviously, this effect is related to the out-of-plane sample dimension (so that it tends to diminish for increasing sample thickness), and has been found to be relevant with reference to the geometrical setting employed by Desrues & Hammad (1989), in which the sample is 350 mm × 100 mm, with a thickness of 35 mm.

A comparison between results obtained allowing for the out-of-plane compliance (dashed line) and neglecting it (solid line) is shown in Fig. 14, for two values of confining pressure, $p'_0 = 100$ and 400 kPa. Although the qualitative behaviour and band inclination are not altered, the onset of strain localisation occurs at a significantly larger axial strain (about 0·5–1·0% larger) when out-of-plane compliance is taken into account, and this brings the simulations closer to the experimental results obtained by Desrues & Hammad (1989) and reported in Fig. 15. We note that the axial strain at localisation is almost perfectly matched. The effect of the out-of-plane compliance increases as the confining pressure increases.

The out-of-plane compliance also delays the appearance of band saturation for dense sand at lower confining pressures. For instance, dense sand with $e_0 = 0{\cdot}673$ at a confining pressure of $p'_0 = 20$ kPa exhibits band saturation

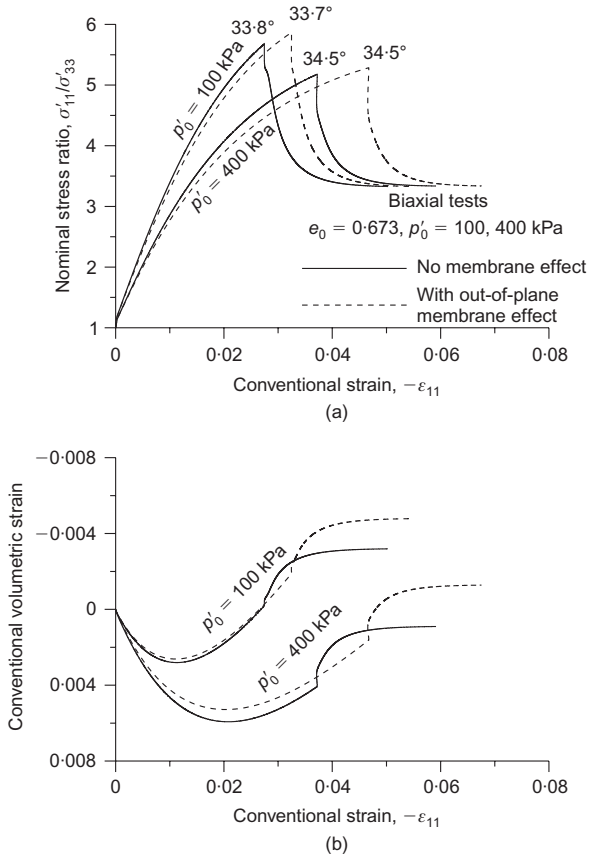

Fig. 14. Biaxial compression of dense sand, effects of out-of-plane stiffness on: (a) nominal stress ratio against conventional axial strain; (b) conventional volumetric strain against axial strain

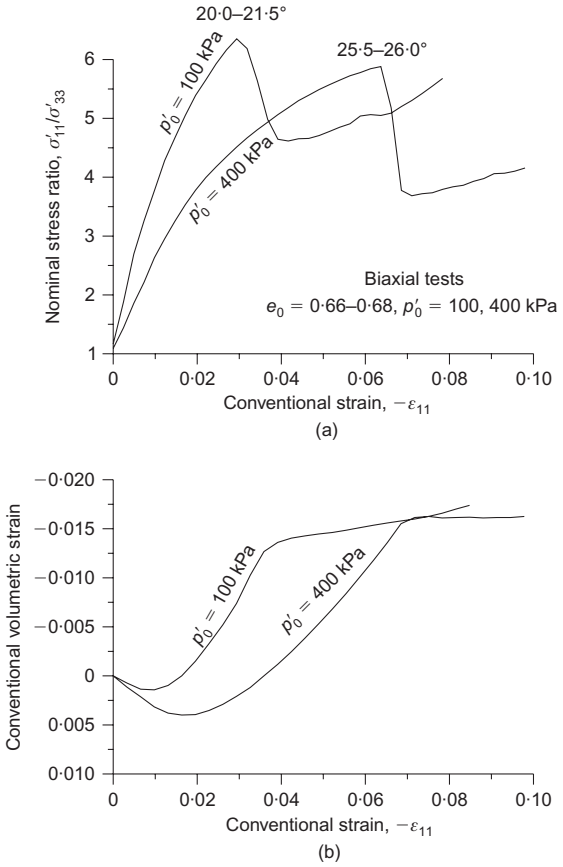

Fig. 15. Experimental results on samples of dense Hostun sand at different confining pressure: (a) nominal axial stress against conventional strain; (b) conventional volumetric against axial strain (from Desrues & Hammad, 1989)

if the out-of-plane compliance is neglected, and does not when the out-of-plane compliance is taken into account. On the other hand, the out-of-plane compliance was found to have only a small effect on band saturation in loose sand: Fig. 16 shows that for $e_0 = 0{\cdot}914$, $p'_0 = 100$ kPa, band saturation occurs at a vertical strain about 0·2% larger when the out-of-plane compliance is considered.

The membrane surrounding the sample has a further effect related to the fact that progression of localised deformation in the post-critical range involves stretching of the membrane, yielding an apparent increase of stiffness. This is an effect that is anticipated by some experiments by Desrues (1984) and confirmed by the fact that Vardoulakis & Graf (1985), using a thicker sample and a thinner membrane than Desrues, find a much less pronounced re-hardening, but it does not appear to have been previously explained quantitatively through mechanical modelling. In order to model the effect, a 0·50 mm thick lateral membrane has been assumed to be stretched under plane stress conditions (because the contact with a granular medium occurs at isolated points and leaves the membrane almost unloaded transversely), and its contribution has been averaged over the sample thickness of 35 mm. The in-plane components of strain are assumed to be equal in the sample and the membrane. The simulations are presented in Fig. 17 (for dense sand $e_0 = 0{\cdot}673$, $p'_0 = 100$, 400 kPa), where the dashed (solid) lines represent results corrected (uncorrected) to take account of the membrane stretching during post-localisation behaviour. The same gentle increase in stress ratio with increasing deformation can be seen in the experimental results of Fig. 15: this is a system response not a material response.

It can be observed that, as expected, the effect of membrane stretching is negligible at the beginning of the post-

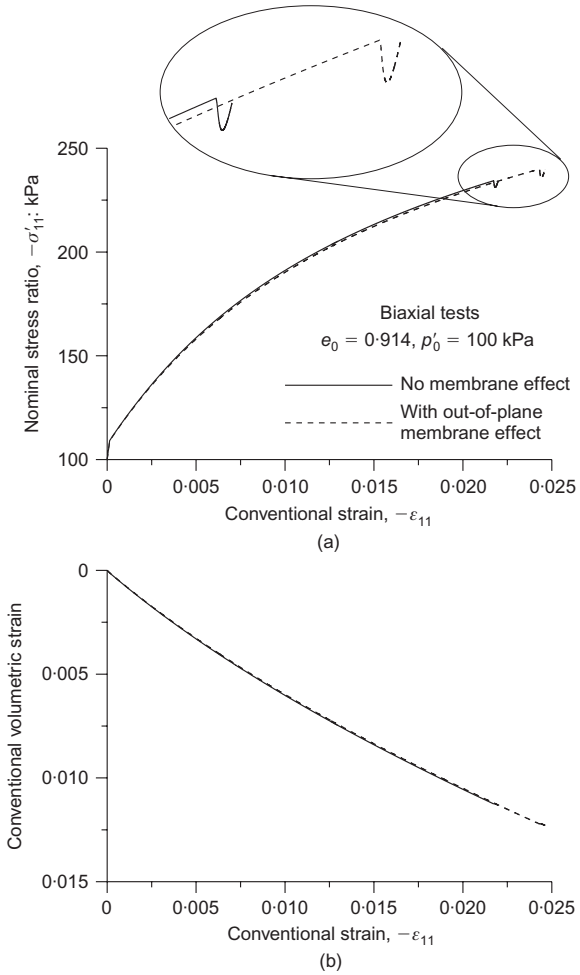

Fig. 16. Biaxial compression of loose sand, effects of out-of-plane compliance on: (a) nominal stress against conventional axial strain; (b) conventional volumetric strain against axial strain

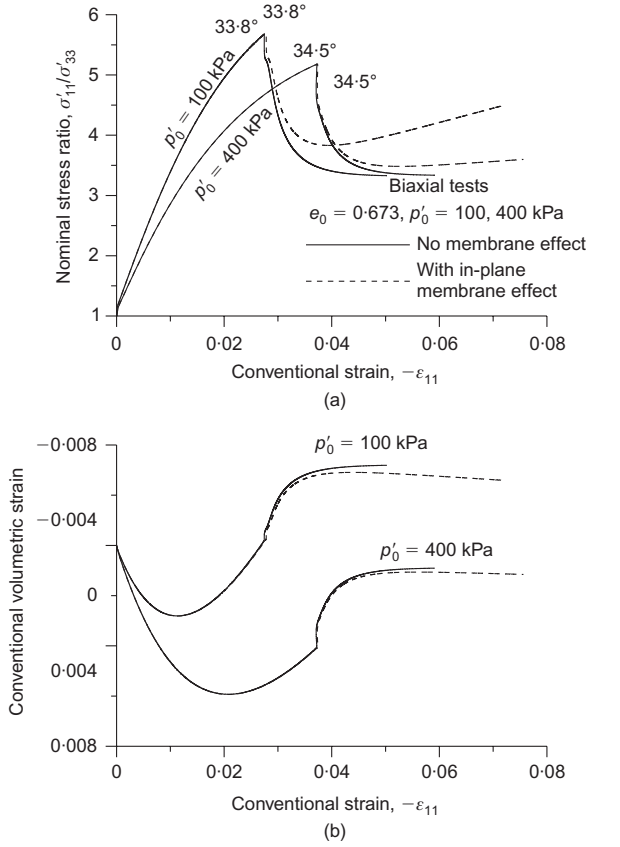

Fig. 17. Increase of apparent stiffness post-localisation due to membrane stretching. Biaxial compression of dense sand: (a) nominal stress ratio against conventional axial strain; (b) conventional volumetric strain against axial strain

localisation behaviour, whereas it becomes later more and more important, leading to an increase of the residual strength that can explain the experimental results obtained by Desrues & Hammad (1989), as shown in Fig. 15(a). The computed slope of the increase of residual strength against conventional vertical strain—the apparent stiffness—is consistent with the measurements, and this is another indication that the assumed band thickness is close to the experimental one (since band thickness strongly influences the contribution of the membrane to the apparent stiffness). The membrane stretching effect becomes negligible at high confining pressures, again as experimentally observed.

Results presented in this section support the idea of a new experimental programme performed on biaxial tests, employing samples of different out-of-plane thickness and membranes of different characteristics. This would permit systematic study of the influence of membrane compliance on localisation and post-localisation behaviour.

CONCLUSIONS

Shear band nucleation, growth and possible saturation have been investigated in relation to the modelling of mechanical behaviour of sand tested in biaxial and triaxial compression and to the characteristics of experimental apparatus. Although not exhaustive, our results show that the use of mathematical tools developed by Gajo *et al.* (2004) allows ready examination of features that have not been previously modelled, but have often been suggested to have a strong influence on experimental results. We have found that some of these features are subtle, in the sense that they do not much alter the homogeneous response of a sample, but strongly affect the occurrence of localisation and/or the post-localisation behaviour, and that these effects may be linked to the detail of the configuration of testing. For instance, elastic anisotropy has a strong effect in promoting strain localisation under triaxial conditions, but this effect is not so pronounced for biaxial states, and the effects on post-localisation behaviour are mainly related to the occurrence of saturation mechanisms at confining pressures smaller than those calculated for elastic isotropy.

Other examples are related to the effects of the membrane, altering the out-of-plane compliance and increasing the stiffness during post-critical deformation mechanisms: again, the localised behaviour is affected much more significantly than the pre-localised, homogeneous response.

These studies indicate the need for further experimental research in a number of areas.

(*a*) Elastic anisotropy has been found to be important. There is thus a need for more detailed characterisation of elastic anisotropy in as wide a range of testing apparatus as possible, including biaxial apparatus, and true triaxial apparatus, and tests involving rotation of principal stress axes, such as hollow cylinder or simple shear. The wider applicability of the hypothesis of strain-dependent evolving anisotropy can then be tested.

(*b*) The simulations indicate the influence that stress level has on post-localisation response and particularly on band saturation. Investigation of the occurrence of this mechanism in the biaxial test, particularly in dense sand at low confining pressure, can follow procedures

similar to those employed by Chambon & Desrues (1986) and Finno *et al.* (1997).

(*c*) It has been shown that there are two quite different ways in which membrane compliance influences the onset of localisation and the post-localisation response. The departure from the intended plane-strain condition that results from membrane compliance leads us to expect that tests on samples of different out-of-plane thickness will show decreasing axial strain at which strain localisation occurs as the sample thickness is increased. On the other hand, the in-plane constraint provided by the membrane leads to an increasing load after the strong softening following sharp band formation in dense sand. This system effect should tend to disappear as the sample (out-of-plane) thickness increases. Some experimental evidence for a certain range of sample sizes is provided by Desrues (1984) and Vardoulakis & Graf (1985).

ACKNOWLEDGEMENTS

Financial support of MIUR-COFIN 2003, protocol no. 2003082105_002 (AG), the MIUR-COFIN 2004, protocol no. 2004083253_002 (DB), and of the UK Engineering and Physical Sciences Research Council (AG and DMW) and of the University of Bristol (DMW) is gratefully acknowledged.

APPENDIX. MATHEMATICAL DETAILS OF THE CONSTITUTIVE MODEL

The constitutive model employed in our study is briefly described (following Gajo *et al.* (2004), where further details and a thorough account of the notation used can be found).

The *state parameter* ψ (Fig. 1(b)) is defined in terms of specific volume v as

$$\psi = v - v_\Lambda + \Lambda \ln p' \tag{3}$$

where v_Λ and Λ are positive constitutive parameters.

An isotropic yield function (Fig. 1(a)) is assumed to depend on the set of internal variables $\gamma^{\mathrm{p}}_{\mathrm{oct}}$ and $\mathrm{tr}\boldsymbol{\varepsilon}^{\mathrm{p}}$ and effective stress $\boldsymbol{\sigma}'$ in the form

$$f\left(\boldsymbol{\sigma}', \gamma^{\mathrm{p}}_{\mathrm{oct}}, \mathrm{tr}\boldsymbol{\varepsilon}^{\mathrm{p}}\right) = \sqrt{J_{2(\sigma)}} - (1 - k\psi)\, g\left(\theta_{(\sigma)}\right) M\, s\left(\gamma^{\mathrm{p}}_{\mathrm{oct}}\right) p' \tag{4}$$

where $J_{2(\sigma)} = (\mathrm{dev}\ \boldsymbol{\sigma} \cdot \mathrm{dev}\ \boldsymbol{\sigma})/2$ is the second invariant of the stress tensor

$$M = \frac{2\sqrt{3}\sin\phi_{\mathrm{cs}}}{3 - \sin\phi_{\mathrm{cs}}} \tag{5}$$

k and ϕ_{cs} are positive constitutive parameters, the function

$$g\left(\theta_{(\sigma)}\right) = \frac{2m}{1 + m + (1 - m)\cos 3\theta_{(\sigma)}} \tag{6}$$

defines the deviatoric section of the yield surface as a function of the Lode angle, $\theta_{(\sigma)}$, and of the ratio between the strengths in triaxial extension and compression, m (see Fig. 1(c)) (taken as in Argyris *et al.*, 1974). The internal variable $\gamma^{\mathrm{p}}_{\mathrm{oct}}$ is the accumulated octahedral plastic strain

$$\gamma^{\mathrm{p}}_{\mathrm{oct}} = \int_{\text{deformation path}} \sqrt{\tfrac{1}{3}\,\mathrm{dev}\,\dot{\boldsymbol{\varepsilon}}^{\mathrm{p}} \cdot \mathrm{dev}\,\dot{\boldsymbol{\varepsilon}}^{\mathrm{p}}} \tag{7}$$

which is used to describe the smooth degradation of stiffness with progressive deformation, through the following hyperbolic relationship (Fig. 1(e)), inspired by an equivalent function defined by Gajo & Muir Wood (1999a, 1999b)

$$s\left(\gamma^{\mathrm{p}}_{\mathrm{oct}}\right) = 1 - \frac{B}{B/(1 - R) + \gamma^{\mathrm{p}}_{\mathrm{oct}}} \tag{8}$$

where the constitutive parameters $R < 1$ and B define respectively the initial angular opening of the yield surface and the stiffness of plastic response. When $s(\gamma^{\mathrm{p}}_{\mathrm{oct}}) = 1$, equation (4) represents the peak strength surface sketched in Fig. 1(c). Note that the yield surface (an open, non-circular cone in stress space, with an angular opening depending on ψ and $\gamma^{\mathrm{p}}_{\mathrm{oct}}$, Fig. 1(a)) tends to the peak strength surface when $\gamma^{\mathrm{p}}_{\mathrm{oct}}$ increases.

The evolution of elastic anisotropy is described assuming that the complementary free-energy density depends not only on the stress $\boldsymbol{\sigma}$, but also on the history of plastic deformation. Assuming hyperelasticity (of the elastic part of the deformation), the tangent stiffness is given by

$$\mathbb{E} = \lambda\, \mathbf{B} \otimes \mathbf{B} + 2\mu\, \mathbf{B} \mathbin{\overline{\otimes}} \mathbf{B} \tag{9}$$

where λ and μ are elastic constants playing a role similar to the Lamé coefficients of isotropic elasticity and $\mathbf{B}$ is a symmetric, second-order, positive definite fabric tensor, subject to the constraint

$$\mathrm{tr}\mathbf{B}^2 = 3 \tag{10}$$

describing fabric anisotropy and depending on the plastic strain $\boldsymbol{\varepsilon}^{\mathrm{p}}$. Tensor $\mathbf{B}$ is assumed to evolve with plastic distortional strain (Gajo *et al.*, 2004):

$$B = -\beta\, \mathrm{dev}\,\boldsymbol{\varepsilon}^{\mathrm{p}} + \sqrt{\frac{3 - 2J_{2(\varepsilon^{\mathrm{p}})}\beta^2}{3}}\, \mathbf{I} \tag{11}$$

where the function $\beta = \beta(J_{2(\varepsilon^{\mathrm{p}})}, \theta_{(\varepsilon^{\mathrm{p}})})$ depends on the plastic strain (through its second invariant $J_{2(\varepsilon^{\mathrm{p}})}$ and Lode angle $\theta_{(\varepsilon^{\mathrm{p}})}$) according to the law

$$\beta\left(J_{2(\varepsilon^{\mathrm{p}})}, \theta_{(\varepsilon^{\mathrm{p}})}\right) = \frac{A_\varepsilon\, g\left(\theta_{(\varepsilon^{\mathrm{p}})}\right)}{B_\varepsilon\, g\left(\theta_{(\varepsilon^{\mathrm{p}})}\right) + \sqrt{2J_{2(\varepsilon^{\mathrm{p}})}}} \tag{12}$$

and A_ε, m_ε, contained in $g(\theta_{(\varepsilon^{\mathrm{p}})})$ (which is exactly equivalent to the deviatoric strength function $g(\theta_{(\sigma)})$, equation (6), but with the stress replaced by plastic strain), and B_ε, (Fig. 3) are non-negative constitutive parameters defining the asymptotic value of elastic anisotropy and the rate at which anisotropy evolves with increasing distortional plastic strain. Note that, at zero deviatoric plastic strain, the elastic anisotropy is zero and $\mathbf{B} = \mathbf{I}$, whereas at very large deviatoric plastic strains, the fabric tensor $\mathbf{B}$ reaches the asymptotic condition (Fig. 3(b)).

The rate form of constitutive equations can be written as

$$\dot{\boldsymbol{\sigma}}' = \mathbb{E}[\dot{\boldsymbol{\varepsilon}} - \dot{\boldsymbol{\varepsilon}}^{p}] + \mathbb{H}[\dot{\mathbf{B}}] \tag{13}$$

where

$$\dot{\mathbf{B}} = \frac{\partial \mathbf{B}}{\partial \boldsymbol{\varepsilon}^{\mathrm{p}}}[\boldsymbol{\varepsilon}^{p}] \tag{14}$$

and the fourth-order tensor $\partial\mathbf{B}/\partial\boldsymbol{\varepsilon}^{\mathrm{p}}$ is given by Gajo *et al.* (2004). Tensor $\mathbb{H}$ appearing in equation (13) originates from elastoplastic coupling as

$$\begin{aligned}\mathbb{H} = {} & \lambda\left[\mathbf{B} \otimes (\boldsymbol{\varepsilon} - \boldsymbol{\varepsilon}^{\mathrm{p}}) + \mathbf{B} \cdot (\boldsymbol{\varepsilon} - \boldsymbol{\varepsilon}^{\mathrm{p}})\, \mathbf{I} \mathbin{\overline{\otimes}} \mathbf{I}\right] \\ & + 2\mu\left[\mathbf{B}(\boldsymbol{\varepsilon} - \boldsymbol{\varepsilon}^{\mathrm{p}}) \mathbin{\overline{\otimes}} \mathbf{I} + \mathbf{I} \mathbin{\overline{\otimes}} \mathbf{B}(\boldsymbol{\varepsilon} - \boldsymbol{\varepsilon}^{\mathrm{p}})\right]\end{aligned} \tag{15}$$

As a result, from equation (13), the rate of strain may be understood as the sum of a reversible $\mathbb{E}^{-1}[\dot{\boldsymbol{\sigma}}']$ and an irreversible strain rate $\dot{\boldsymbol{\varepsilon}}^{\mathrm{i}}$, the latter linked to the plastic strain rate $\dot{\boldsymbol{\varepsilon}}^{\mathrm{p}}$ by

$$\dot{\boldsymbol{\varepsilon}}^{\mathrm{i}} = \mathbb{G}[\dot{\boldsymbol{\varepsilon}}^{\mathrm{p}}] \tag{16}$$

where the coupling fourth-order tensor $\mathbb{G}$ is defined as

$$\mathbb{G} = \mathbf{I} \mathbin{\overline{\otimes}} \mathbf{I} - \mathbb{E}^{-1}\mathbb{H}\frac{\partial \mathbf{B}}{\partial \boldsymbol{\varepsilon}^{\mathrm{p}}} \tag{17}$$

The rate of irreversible deformation is governed by

$$\dot{\boldsymbol{\varepsilon}}^{\mathrm{i}} = \dot{\gamma}\mathbf{P} \tag{18}$$

where $\dot{\gamma} \geqslant 0$ is the plastic multiplier and $\mathbf{P}$ is the (symmetric) flow mode tensor. For simplicity we use deviatoric associativity and, following Gajo & Muir Wood (1999a, b), we assume that the plastic dilatancy is governed by a Cam-clay type flow rule (Fig. 1(f))

$$\frac{\mathrm{tr}\,\mathbf{P}}{|||\mathrm{dev}\,\mathbf{P}|||} = -\sqrt{3}A\left[(1 + k_{\mathrm{d}}\psi)M - \frac{\sqrt{J_{2(\sigma)}}}{g\left(\theta_{(\sigma)}\right)p'}\right] \tag{19}$$

where A and k_{d} are constitutive parameters. Equation (19) completely defines the tensor $\mathbf{P}$.

Prager's consistency condition yields the elasto-plastic incremental constitutive laws

$$\dot{\boldsymbol{\sigma}'} = \mathbb{E}[\dot{\boldsymbol{\varepsilon}}] - \frac{\langle \mathbf{Q} \cdot [\dot{\boldsymbol{\varepsilon}}] \rangle}{H + \mathbf{Q} \cdot \mathbb{E}[\mathbf{P}]} \mathbb{E}[\mathbf{P}] \tag{20}$$

in which H is the hardening modulus, $\langle\rangle$ is the Macaulay brackets operator and

$$\mathbf{Q} = \frac{\partial f}{\partial \boldsymbol{\sigma}'} \tag{21}$$

is the yield function gradient.

REFERENCES

Argyris, J. H., Faust, G., Szimmat, J., Warnke, P. & Willam, K. (1974). Recent developments in the finite element analysis of prestressed concrete reactor vessels. *Nuc. Eng. Des*. **28**, 42–75.

Been, K. & Jefferies, M. J. (1985). A state parameter for sands. *Géotechnique* **35**, No. 1, 99–112.

Bigoni, D. & Loret, B. (1999). Effects of elastic anisotropy on strain localization and flutter instability in plastic solids. *J. Mech. Phys. Solids* **47**, No. 7, 1409–1436.

Bigoni, D., Loret, B. & Radi, E. (2000). Localization of deformation in plane elastic-plastic solids with anisotropic elasticity. *J. Mech. Phys. Solids* **48**, Nos 6–7, 1441–1466.

Chambon, R. & Desrues, J. (1986). Discussion on 'Comparison of frictional material models with respect to shear band initiation' (by F. Molenkamp). *Géotechnique* **36**, No. 1, 133–135.

Desrues, J. (1984). *La localisation de la deformation dans les materiaux granulaires*. Thèse de Doctorat es Science, USMG and INPG, Grenoble, France.

Desrues, J. & Hammad, W. (1989). Shear band dependency on mean stress level. In *Numerical methods for localisation and bifurcation of granular materials* (eds E. Dembicki, G. Gudehus and Z. Sikora), pp. 57–67. Gdansk: Technical University of Gdansk.

Desrues, J., Chambon, R., Mokni, M. & Mazerolle, F. (1996). Void ratio evolution inside shear bands in triaxial sand specimens studied by computed tomography. *Géotechnique* **46**, No. 3, 529–546.

Desrues, J. & Viggiani G. (2004). Strain localization in sand: an overview of the experimental results obtained in Grenoble using stereophotogrammetry. *Int. J. Numer. Anal. Methods Geomech.* **28**, No. 4, 279–321.

Drescher, A. & de Josselin de Jong, G. (1972). Photoelastic verification of a mechanical model for the flow of a granular material. *J. Mech. Phys. Solids* **20**, 337–351.

Finno, R. J., Harris, W. W., Mooney, M. A. & Viggiani, G. (1997). Shear bands in plane strain compression of loose sand. *Géotechnique* **47**, No. 1, 149–165.

Gajo, A. (2003). *Instability phenomena in sand samples*. PhD thesis, University of Bristol.

Gajo, A. (2004). The influence of system compliance on collapse of triaxial sand samples. *Can. Geotech. J.* **41**, No. 2, 257–273.

Gajo, A. & Muir Wood, D. (1999a). A kinematic hardening constitutive model for sands: the multiaxial formulation. *Int. J. Numer. Anal. Methods Geomech.* **23**, No. 5, 925–965.

Gajo, A. & Muir Wood, D. (1999b). Severn-Trent sand: a kinematic hardening constitutive model for sands: the q–p formulation. *Géotechnique* **49**, No. 5, 595–614.

Gajo, A., Bigoni, D. & Muir Wood, D. (2001). Stress induced elastic anisotropy and strain localisation in sand. In *Bifurcation and localisation theory in geomechanics* (eds H. B. Muhlhaus, A. Dyskin and E. Pasternak), pp. 37–44. Lisse: Swets & Zeitlinger.

Gajo, A., Bigoni, D. & Muir Wood, D. (2004). Multiple shear band development and related instabilities in granular materials. *J. Mech. Phys. Solids* **52**, No. 12, 2683–2724.

Hardin, B. O. & Black, W. L. (1968). Vibration modulus of normally consolidated clay. *J. Soil Mech. Found. Div. ASCE* **94**, No. SM2, 353–369.

Houlsby, G. T. (1985). The use of a variable shear modulus in elastic-plastic models for clays. *Comput. Geotech.* **1**, No. 3, 3–13.

Hueckel, T. & Maier, G. (1977). Incremental boundary value problems in the presence of coupling of elastic and plastic deformations: a rock mechanics oriented theory. *Int. J. Solids Struct.* **13**, No. 1, 1–15.

Muir Wood, D. (2002). Some observations of volumetric instabilities in soils. *Int. J. Solids Struct.* **39**, No. 13–14, 3429–3449.

Muir Wood, D., Lings, M. L., Nash, D. F. T. & Gajo, A. (2001). Anisotropy of soils: laboratory measurements and constitutive implementation. *Proc. 15th Int. Conf. Soil Mech. Geotech. Engng, Istanbul* **1**, 321–324.

Roscoe, K. H. (1970). The influence of strains in soil mechanics: 10th Rankine Lecture. *Géotechnique* **20**, No. 2, 129–170.

Tatsuoka, F., Nakamura, S., Huang, C. & Tani, K. (1990). Strength anisotropy and shear band direction in plane strain tests of sand. *Soils Found.* **30**, No. 1, 35–54.

Vardoulakis, I. & Graf, B. (1985). Calibration of constitutive models for granular materials using data from biaxial experiments. *Géotechnique* **35**, No. 3, 299–317.

Vardoulakis, I. & Sulem, J. (1995). *Bifurcation analysis in geomechanics*. Glasgow: Blackie Academic and Professional.

Wroth, C. P. & Bassett, R. H. (1965). A stress–strain relationship for the shearing behaviour of a sand. *Géotechnique* **15**, No. 1, 32–56.